

Effects of spatial confinement and layer disorder in photoluminescence of $\text{GaAs}_{1-x}\text{Bi}_x/\text{GaAs}$ heterostructures

This content has been downloaded from IOPscience. Please scroll down to see the full text.

2013 J. Phys. D: Appl. Phys. 46 065306

(<http://iopscience.iop.org/0022-3727/46/6/065306>)

View [the table of contents for this issue](#), or go to the [journal homepage](#) for more

Download details:

IP Address: 142.104.83.231

This content was downloaded on 20/04/2016 at 19:13

Please note that [terms and conditions apply](#).

Effects of spatial confinement and layer disorder in photoluminescence of GaAs_{1-x}Bi_x/GaAs heterostructures

Yu I Mazur¹, V G Dorogan¹, M Benamara¹, M E Ware¹, M Schmidbauer², G G Tarasov³, S R Johnson⁴, X Lu^{4,7}, S-Q Yu⁵, T Tiedje⁶ and G J Salamo¹

¹ Institute for Nanoscience and Engineering, University of Arkansas, 731 W. Dickson str., Fayetteville, AR 72701, USA

² Leibniz-Institute for Crystal Growth, Max-Born-Str. 2, D-12489 Berlin, Germany

³ Institute of Semiconductor Physics, National Academy of Sciences of Ukraine, pr. Nauki 45, Kyiv 03028, Ukraine

⁴ Department of Electrical Engineering, Arizona State University, Tempe, AZ 85287, USA

⁵ Department of Electrical Engineering, University of Arkansas, 3217 Bell Engineering, Fayetteville, AR 72701, USA

⁶ Department of Electrical and Computer Engineering, University of Victoria, Victoria, British Columbia V8W 3P6, Canada

E-mail: ymazur@uark.edu (Yu I Mazur)

Received 19 September 2012, in final form 4 November 2012

Published 10 January 2013

Online at stacks.iop.org/JPhysD/46/065306

Abstract

The structural and optical properties of a set of high-quality GaAs_{1-x}Bi_x/GaAs quantum well (QW) heterostructures with Bi concentrations ranging from 3.5% to 6.7% are studied. The energies of the excitonic ground state transitions are determined as a function of Bi concentration and spatial confinement. The influence of material disorder on the optical properties of QWs is investigated. It is determined that trap-related luminescence responds differently to temperature changes depending on whether the Bi concentration is more or less than 5%. Below 5% it contributes significantly to the overall photoluminescence line shape whereas above 5%, it is insignificant.

(Some figures may appear in colour only in the online journal)

1. Introduction

Dilute bismides GaAs_{1-x}Bi_x have great potential for optical device applications in the near and mid-infrared regions as well as electronic devices for spintronics [1, 2]. There are three material properties that are mainly responsible for this potential: (i) a large band gap reduction caused by Bi incorporation in GaAs (up to ~90 meV/% of Bi) that perturbs mainly the valence band, (ii) a strong spin-orbit splitting enhancement that can be tailored by isoelectronic doping and (iii) a temperature insensitive band gap. Recently, important progress has been made in the growth of GaAs_{1-x}Bi_x by molecular-beam epitaxy (MBE). Single quantum wells

(QWs) and multiple QW structures of good structural quality and strong photoluminescence (PL) have been demonstrated without the need for post-growth annealing [2–4]. In spite of this progress many questions are still open regarding the physics of dilute bismides, for example, ‘what is the origin of the observed strong band gap reduction caused by Bi incorporation?’, ‘what is the character of impurity distribution?’ and ‘what mechanisms affect PL emission?’ [5–8]. The most recent studies show that Bi distribution in GaAs_{1-x}Bi_x is more complicated than simply a random distribution with alloy clustering. Mechanisms such as phase separation, atomic ordering and even Bi droplet formation must be considered in the bismide family depending on the Bi concentration range [9–13]. These effects have a significant influence on the optical and electrical properties of the resulting semiconductor alloys.

⁷ Current address: Varian Semiconductor Equipment, Applied Materials, Gloucester, MA, 01930, USA.

In our recent paper [14], we reported the results of a PL study of an 11 nm thick GaAs_{0.94}Bi_{0.06} layer embedded in GaAs and grown by MBE at a low temperature. In this layer we observed a peculiar structure of the emission spectrum for high excitation density, which was attributed to evolution of the QW excited states. Low-temperature PL exhibited a pronounced blueshift both with temperature and excitation intensity, which was attributed to the defect-controlled radiative recombination of localized excitons. Although carrier localizations in the GaAs_{1-x}Bi_x epilayers have been extensively discussed [2, 15, 16], detailed data on PL are still important for understanding the carrier dynamics in the regions of concentration fluctuations including clustering of Bi atoms. In this study, we analyse the effect of spatial confinement on the optical properties of GaAs_{1-x}Bi_x using GaAs as a barrier material, and the influence of disorder in the QW on its optical properties.

2. Sample structure characterization

The heterostructures studied in this work are grown on semi-insulating GaAs (1 0 0) substrates in a VG V80H solid source MBE system following the technique described in [2]. They include a 300 nm thick GaAs buffer layer, a thin GaAs_{1-x}Bi_x layer and a nominally 30 nm thick GaAs capping layer. The GaAs_{1-x}Bi_x epilayers are deposited at a reduced growth rate ($\sim 1 \text{ nm min}^{-1}$), low substrate temperature (280–320 °C) and low As₂ overpressure (As₂/Ga ~ 1) compared with the usual GaAs growth conditions. The incorporation of Bi is determined by the As₂ flux, Bi flux and growth temperature.

The structural properties of the as-grown samples are characterized using high-resolution x-ray diffraction (HR-XRD). Reciprocal space mapping (not shown here), performed in the vicinity of the (asymmetrical) 224 Bragg reflection, indicates that all the GaAsBi layers are pseudomorphic (coherent) with the GaAs buffer layer with a very low dislocation density. X-ray rocking curves (2θ - ω scans) of the symmetrical (004) Bragg reflections are also recorded for all samples. Figures 1(a) and (b) show these curves for samples 2 (see sample identification below) and 3, respectively, along with each sample's corresponding simulation carried out within the framework of a quasi-kinematical scattering algorithm [14]. These simulations are used to analyse the vertical distribution of Bi inside the GaAsBi QWs, the corresponding vertical strain distribution, and the layer thicknesses of the QW and the GaAs cap layer. These are summarized in table 1. The experimental rocking curves cannot be fit with sufficient accuracy using a single GaAsBi layer with a uniform Bi concentration. This is most likely due to the interdiffusion of Bi and As atoms, which slightly blurs the interfaces surrounding the GaAsBi QW. Therefore, a multilayer model was used in the fitting procedure resulting in a non-constant Bi distribution over the nominal width of the GaAsBi film. From the derived Bi concentration profile (thicknesses, d_i , with corresponding Bi contents x_i) the maximum Bi concentration x_{max} in the GaAsBi QW and

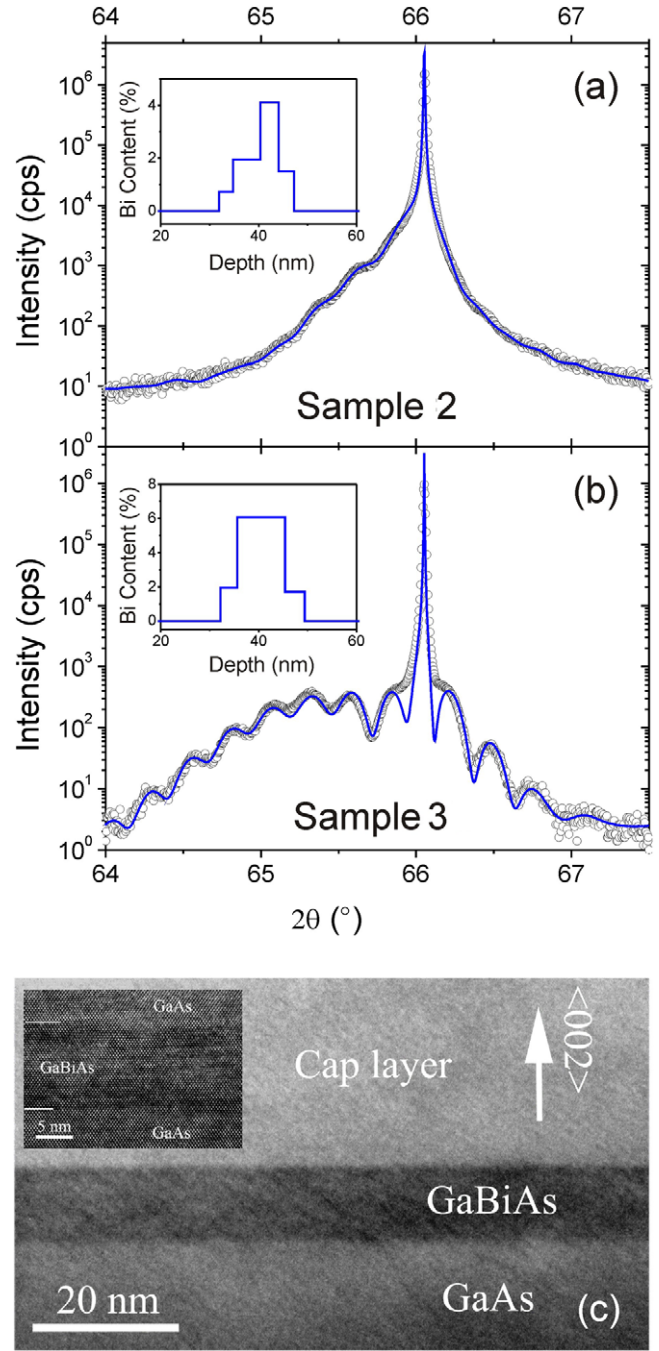


Figure 1. Experimental x-ray rocking curves (O) around the GaAs 004 symmetrical Bragg reflection for (a) sample 2 and (b) sample 3 along with the corresponding simulations (solid lines). The insets show the vertical atomic Bi concentration profiles in the samples used for the simulations. (c) Bright-field TEM image of sample 3 taken under a two-beam condition with (002) reflecting planes. The GaAsBi layer with a constant thickness of 11 nm appears with a dark contrast between the GaAs substrate and the cap layer. Inset: high-resolution TEM image of the well, taken along the $\langle 110 \rangle$ zone axis.

an effective layer thickness d_{QW} as defined by

$$d_{\text{QW}} = \sum_i d_i \frac{x_i}{x_{\text{max}}} \quad (1)$$

were determined within a certain fitting accuracy, as shown in table 1. One can see here that the maximum Bi concentration

Table 1. Characterization of the GaAs_{1-x}Bi_x/GaAs heterostructures.

GaAsBi/ GaAs sample	x_{\max} (%)	d_{QW} (nm)	d_{cap} (nm)	E_{\max} ($T = 15$ K) (eV)	E_{\max} ($T = 295$ K) (eV)
1	3.5 ± 0.2	13.0 ± 0.5	28.2 ± 0.5	1.182	1.132
2	4.1 ± 0.2	7.5 ± 0.5	33 ± 0.5	1.240	1.192
3	6.0 ± 0.2	11.0 ± 0.3	32.0 ± 0.5	1.085	1.037
4	6.5 ± 0.5	11.5 ± 1.0	33.2 ± 0.5	1.055	1.051
5	6.7 ± 0.3	5.6 ± 1.0	31.5 ± 0.5	1.113	1.067

for these samples varies from 3.5% to 6.7% and the layer thickness varies from 5.6 to 13 nm. Such small layer thicknesses indicate that the effects of spatial confinement will transform the layer in a QW structure. Further structural studies by means of transmission electron microscopy (TEM) support this observation.

Cross-section TEM samples are prepared using mechanical polishing followed by ion milling. The TEM measurements are performed at 300 keV in an FEI Titan 80–300 S/TEM fitted with a CEOS image corrector. Figure 1(c) is a bright-field image obtained under two-beam conditions with the (002) reflecting planes for sample 3. The GaAsBi layer appears dark between the GaAs substrate and the cap layer. The layer appears to have a constant thickness of 11 nm without any remarkable disruptions along the sample's length. At the same time, the contrast appears to be very uniform indicating that Bi is incorporated without significant clustering. However, we cannot rule out that the slight contrast variations, which we believe are mainly due to sample preparation artefacts and a resulting amorphous surface layer, might obscure some amount of inhomogeneity of the Bi content. The inset is a high-resolution TEM image of the QW, taken along the $\langle 110 \rangle$ zone axis, which shows that the GaAsBi layer has very good crystalline structure confirming the x-ray measurements. The layer is pseudomorphic with its in-plane lattice parameter strained to that of the underlying GaAs substrate with no observable dislocations. The interfaces on both the upper and lower sides of the layer are smooth and very well defined with a transition region of only 1–2 monolayers. The small contrast variations, which are noticeable within the well, are assumed to be thickness variation artefacts due to sample preparation. The structural QW-like behaviour is now well characterized through HR-XRD and cross-section TEM. However, true QW confinement is best observed through optical measurements of the exciton PL. We will now present these data.

3. Experimental results and discussion

Next, an extensive temperature and excitation dependent PL study is performed on these bismide QW samples. For this purpose, the samples are inserted into a variable temperature, 10–300 K, closed-cycle helium cryostat and excited using the 532 nm line from a double Nd:YAG laser. The laser beam with powers in the range $\sim 10^{-6}$ – 10^2 mW is focused to a spot with a diameter of ~ 20 μm . The PL signal is dispersed using a 0.5 m single-grating monochromator and detected by a LN-cooled OMA V:InGaAs photodiode detector array.

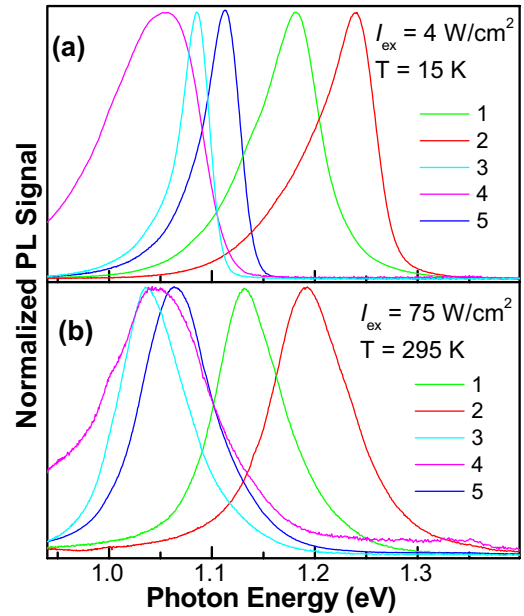


Figure 2. Normalized PL spectra of the samples presented in table 1 for (a) low temperature ($T = 15$ K) and low excitation intensity $I_{\text{ex}} = 4$ W cm^{-2} ; (b) high temperature ($T = 295$ K) and moderate excitation intensity ($I_{\text{ex}} = 75$ W cm^{-2}).

Figure 2 presents the PL spectra of the GaAs_{1-x}Bi_x/GaAs heterostructures measured at low ($T = 15$ K) and high ($T = 295$ K) temperatures for moderate excitation intensities. The spectra are normalized with respect to their PL maxima and the energy positions of these maxima are compiled in table 1. From here it can be seen that when the Bi concentration increases from 3.5% to 6.5%, the low-temperature PL peak redshifts by ~ 180 meV, which is a rate of ~ 60 meV/% Bi. As the temperature increases, the PL peak for each Bi concentration redshifts at different rates; the rate at high temperatures is ~ 54 meV/% Bi. It should be noted that the PL energy depends on the excitation intensity [17]. Therefore, before comparing the PL data from different sources one has to take care to reduce them to similar experimental conditions. The smallest full-width at half-maximum (FWHM), ~ 40 meV, is observed for the PL band located at $E_{\max} = 1.085$ eV. It has been shown in [14] that this PL peak in sample 3 can be assigned to in-well excitonic recombination. Therefore, by comparison, we assign each PL band shown in figure 2 to the exciton ground state emission in its corresponding GaAs_{1-x}Bi_x/GaAs heterostructure. From table 1 we see an irregular dependence of E_{\max} on the Bi concentration, i.e. higher values of x do not always correspond to lower values of E_{\max} as would be

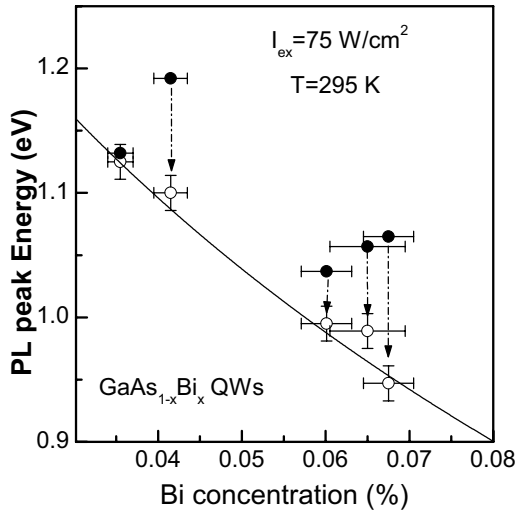


Figure 3. Energies of PL maximum measured in all samples (filled circles) together with experimental error bars determined by the accuracy of determination of the Bi concentration according to table 1. Empty circles show these energies without the effect of spatial confinement. The compositional dependence of $E_{\text{GaAs}_{1-x}\text{Bi}_x}$, given by equation (2) [2], is shown by the solid line.

expected from the bulk bandgap value of the alloy. We attribute these irregularities to the effect of spatial confinement typical of QW structures. In order to take the confinement into account the PL spectra of thick GaAsBi structures ($d_L > 30$ nm), where the effect of confinement is expected to be negligible, are compared with the PL spectra of substantially thinner layers ($d_L < 13$ nm), as in our case. For this comparison, we use the results reported in [2] for GaAsBi samples with $d_L = 30$ – 40 nm. It is found that the room temperature PL energy monotonically decreases with Bi concentration from 1.425 eV for the GaAs band gap down to 0.861 eV for $x = 0.106$ in the $\text{GaAs}_{1-x}\text{Bi}_x$ layer, which is fit perfectly with the relationship

$$E_{\text{GaAs}_{1-x}\text{Bi}_x} = xE_{\text{GaBi}} + (1-x)E_{\text{GaAs}} - bx(1-x), \quad (2)$$

where E_{GaBi} and E_{GaAs} are the bandgap energies of GaBi and GaAs with values of -0.36 eV and 1.425 eV, respectively, and the bowing parameter is given by

$$b = \alpha / (1 + \beta x), \quad (3)$$

with $\alpha = 9.5$ and $\beta = 10.4$.

Equation (2) is plotted in figure 3 as a solid line. In order to calculate the influence of spatial confinement in our heterostructures we approximate it as a finite square well. It should be noted, though, that the cap layer thickness in our samples is only ~ 30 nm, whereas it is 300 nm in [2]. However, it has been shown in [18] that significant deviations from the ‘regular’ QW levels are only expected for very thin cap layers (of the order of about 10 nm). So, we assume that both sets of samples are not influenced by a limited capping layer. We also use for an estimation of confinement an analytical expression derived in [19], which gives a very close approximation of the experimentally observed ground state energy level in the QW structures:

$$E_1 = \Delta E / 2 - \pi^2 \hbar^2 / (4m^* \tilde{d}_L^2). \quad (4)$$

Equation (4) contains the band offset ΔE , the carrier effective mass m^* and an effective well thickness \tilde{d}_L which is defined by

$$\tilde{d}_L = d_L \left\{ \left(1 + \frac{32\Delta E^2 d_L^4}{\pi^6 \hbar^4 m^{*2}} \right)^{1/2} - 1 \right\}^{-1/2}. \quad (5)$$

with d_L being the QW geometrical thickness.

Following [1] we assume that Bi incorporation in the GaAs host material influences only the valence band, leaving the conduction band only slightly perturbed. In this case equation (2) allows us to determine the valence band offset as $\Delta E = E_{\text{GaAs}} - E_{\text{GaAs}_{1-x}\text{Bi}_x}$ and to calculate the ground state energy level E_1 with respect to the QW bandgap energy. Figure 3 shows the energies of PL maxima measured in all samples (filled circles). The energy of the PL maximum from each QW is determined by the Bi concentration and the QW width. The Bi content gradually changes according to the x-ray results in table 1. Therefore, the position of the PL maximum in figure 3 is shown together with experimental error bars, the length of which is determined by the accuracy of determination of the Bi concentration as established in table 1. Empty circles show these energies if the effect of spatial confinement is subtracted taking into account the effective layer thickness given by equation (5). Vertical bars for empty circles show the accuracy of PL energy determination due to the accuracy of d_{QW} in table 1. As can be seen, the PL energies, adjusted to remove the effect due to confinement, fit the alloy bandgap energy dependence on composition quite well. The largest deviation from the solid line in figure 3 is found for the adjusted PL energy of sample 4 ($x = 0.065$), which has the largest uncertainty in Bi concentration (see table 1). Nevertheless, the range of the error bars still comes quite close to the calculated bandgap energy. We thus conclude that the origin of the observed PL spectra in these structures is the confined exciton ground state emission in the $\text{GaAs}_{1-x}\text{Bi}_x/\text{GaAs}$ QW.

Recent studies have shown that GaAsBi films grown on GaAs have a significant amount of disorder, and at the same time that the physical properties of these low Bi concentration bismides change substantially with Bi concentration [11, 16, 20]. It was established that the exciton reduced mass in $\text{GaAs}_{1-x}\text{Bi}_x$ has an unusual compositional dependence. With increasing x , the reduced mass anomalously increases for $x < 5\%$, reaches a maximum, then for $x > 5\%$ it decreases and follows a conventional behaviour [16]. In the low-concentration ‘anomalous’ region acceptor states due to Bi were discovered [11]. The incorporation of Bi in GaAs reduces the density of Ga and/or As-related defects, but introduces Bi-induced defects [20]. The resulting disorder influences the optical properties of GaAsBi compounds significantly, especially at low temperatures and low excitation intensities.

Here, we would like to understand whether this disorder is a factor in our QW samples, by studying the exciton ground state emission. Figure 4 shows the temperature-dependent PL spectra measured in samples 1 and 3 under two different excitation intensities. For $I_{\text{ex}} = 4 \text{ W cm}^{-2}$ the temperature range from 20 to 300 K was scanned in steps of 10 K (figures 4(a) and (c)), whereas for $I_{\text{ex}} = 0.022 \text{ W cm}^{-2}$ the temperature was varied from 20 to 160 K with the same step size (figures

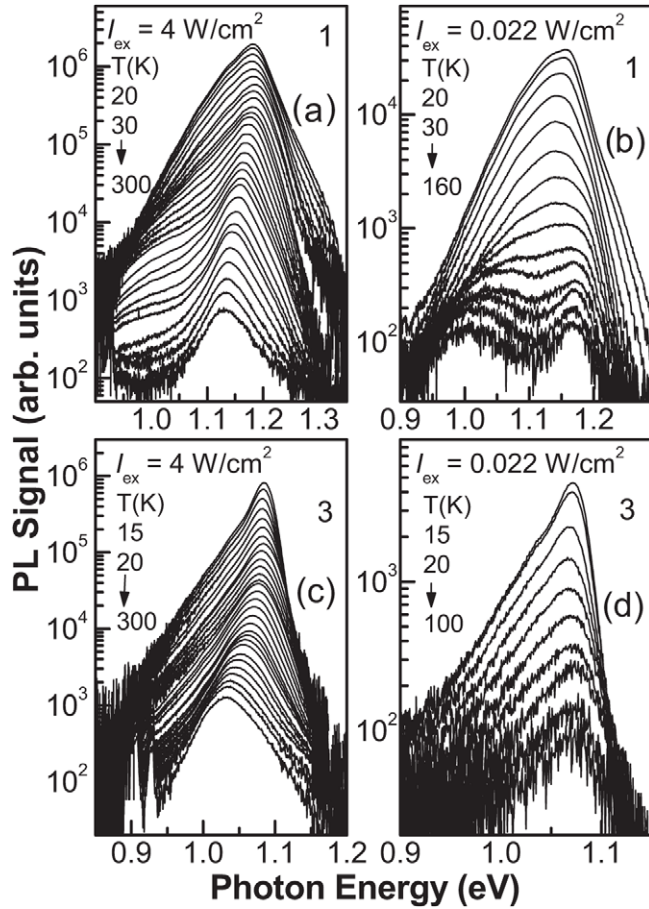


Figure 4. PL spectra respectively from samples 1 and 3 under two different excitation intensities and varying temperature. For $I_{\text{ex}} = 4 \text{ W cm}^{-2}$ the temperature range from 20 to 300 K was scanned in steps of 10 K in (a) and (c), whereas for $I_{\text{ex}} = 0.022 \text{ W cm}^{-2}$ the temperature was varied from 20 to 160 K with the same step size in (b) and (d). In all parts the temperature grows from top to bottom.

4(b) and (d)). In all parts of figure 4 the temperature increases from top to bottom. For $I_{\text{ex}} = 4 \text{ W cm}^{-2}$ the measured PL peak clearly demonstrates a pronounced redshift with temperature increase in both samples. The behaviour of the PL line shape, however, differs significantly between samples 1 and 3. A distinct hump develops in the low-energy tail of the PL band in sample 1 at higher temperatures. In order to resolve this PL structure we examine the low excitation intensity data at $I_{\text{ex}} = 0.022 \text{ W cm}^{-2}$ in more detail.

Figure 5 shows some of the temperature-dependent PL spectra of samples 1 and 3 measured at $I_{\text{ex}} = 0.022 \text{ W cm}^{-2}$. Here, they are normalized to the PL band maximum in each, vertically shifted for clarity, and plotted with the origin taken at the energy of the PL maximum of the high-energy band. Now, the difference in the temperature-dependent behaviour of the PL spectra in samples 1 and 3 becomes more transparent. Inasmuch as the low-energy tail of the PL band in sample 1 transforms obviously into a separate Gaussian-like band, figure 5(b), the low-energy tail of the PL band in sample 3 preserves its exponential shape up to the highest temperatures, figure 5(a). These differences indicate different types of defects fundamentally, which are visible

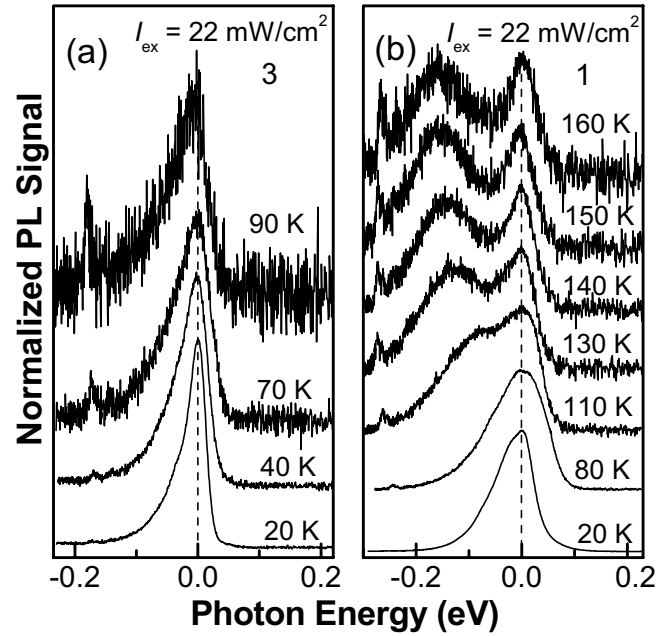


Figure 5. Temperature-dependent PL spectra of samples 3 (a) and 1 (b) measured at $I_{\text{ex}} = 0.022 \text{ W cm}^{-2}$. The spectra are normalized to the PL band maximum in each, vertically shifted for clarity, and plotted with the origin taken at the energy of PL maximum of the high-energy band.

in the PL from samples 1 and 3. Sample 2 very closely resembles the behaviour of sample 1, i.e. two bands appear at higher temperatures with low excitation power. In the same fashion, we can make a direct comparison between sample 3 and samples 4 and 5, i.e. they all exhibit a single band at all temperatures with an exponential tail to lower energy. Comparing all the samples under investigation we find some common features. The Bi concentration in samples 1 and 2 is lower than 5%, whereas in samples 3–5 it exceeds 5%. Thus, we conclude, similar to [16] that the character of the defects forming the PL band line shape in the $\text{GaAs}_{1-x}\text{Bi}_x/\text{GaAs}$ QW structures changes significantly when x leaves the ‘anomalous’ low-concentration region and enters the region of conventional behaviour of reduced exciton mass.

As can be seen in figures 4(a) and (c) the measured PL peak demonstrates a so-called S-shaped shift with increasing temperature from 20 to 300 K. Such behaviour is typical of disordered semiconductors [21]. Figure 6 shows the dependence of the main PL peak energies on temperature under various excitation intensities in samples 1 and 2. At a low excitation intensity a significant deviation from the Varshni equation [22] is observed. This is given by

$$E_g(T) = E_0 - \frac{\alpha T^2}{T + \beta}, \quad (6)$$

where $E_0 = 1.220 \text{ eV}$, $\alpha = 4.9 \times 10^{-4}$ and $\beta = 270 \text{ K}$, which is shown in figure 6(a) by a solid line. It is seen in figures 6(a) and (b) that for increasing excitation intensities the S-shape becomes less noticeable, and for $I_{\text{ex}} = 1 \text{ kW cm}^{-2}$ it has mostly vanished. The temperature dependence of the PL peak energy for this high excitation case more closely

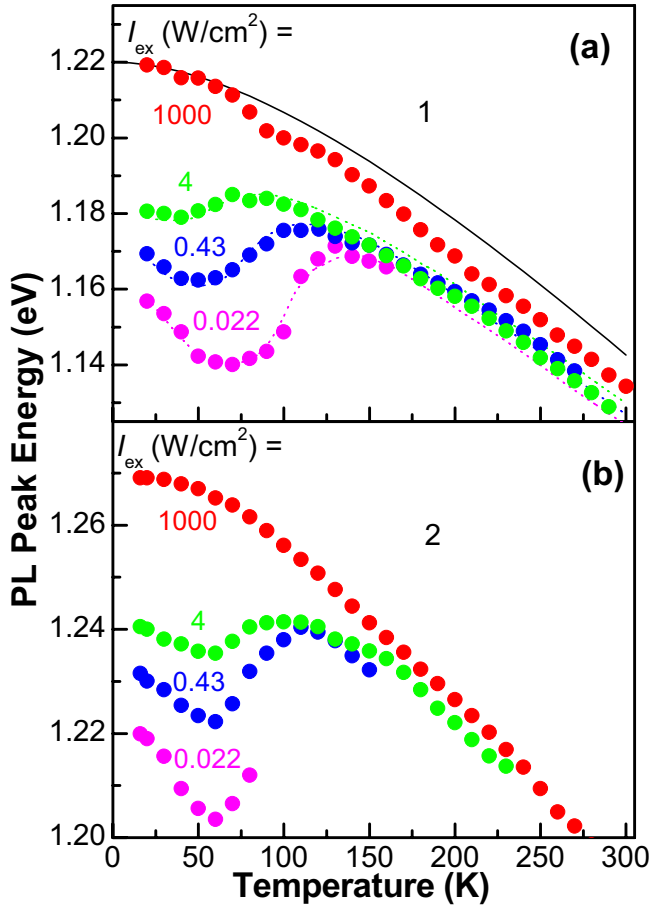


Figure 6. Temperature dependence of the PL peak position with various excitation intensities for (a) sample 1 and (b) sample 2. At a low excitation intensity a significant deviation from the Varshni equation [21] is observed. A fit to the Varshni law, equation (6), with $E_0 = 1.220$ eV, $\alpha = 4.9 \times 10^{-4}$ and $\beta = 270$ K is shown in (a) by the solid line. Theoretical calculations based on rate equations are shown by the dotted lines in (a).

follows equation (6). The S-shaped dependence seen in the low-intensity PL spectra of samples 1 and 2 can be related to the existence of two separate PL peaks with different temperature dependences, as in figure 5(b) [23, 24]. The higher energy peak dominates at low temperatures and remains in the PL spectra at high temperatures. We attribute this peak to the interband exciton recombination in the GaAs_{1-x}Bi_x/GaAs QW. The lower energy peak is strongly temperature dependent, and for low excitation intensities it redshifts relative to the exciton peak with increasing temperature and becomes equal in amplitude at high temperatures. We attribute this behaviour to impurity-induced bound states. Therefore, the S-shaped temperature dependence can be explained by the sharing of PL intensity by the excitonic band and the impurity band.

Another potential source of the peculiar S-shaped temperature dependence is the relaxation of excitons in the presence of trapping centres generated by defects. Hot, free excitons created in the QW relax to the band edge and before radiative recombination can be trapped by various defects. Potential fluctuations caused by varying Bi concentration in the GaAsBi alloys are represented by the randomly distributed sites with a large localization length. The corresponding

density of states (DOS) is described by a Gaussian. In addition to the random sites there may exist Bi clusters that can also serve as localizing centres for excitons. As a result, the exciton dynamics in the GaAsBi alloys can follow the two-scale model developed in [15]. According to this model, the exciton performs transitions between the sites of the first energy scale $\varepsilon_1 = 45$ meV, reflecting the alloy disorder. The exciton can also be transferred to the second energy scale $\varepsilon_2 = 11$ meV where it starts hopping among the cluster sites. The model requires numerical solution using a kinetic Monte Carlo algorithm [15]. Here we propose an alternative model using rate equations that explicitly introduces the filling effect for the impurity states [25–28].

In the framework of our model we assume that at low temperatures excitons are randomly distributed among the defect sites and the distribution is thermodynamically unstable. As a result of heating, weakly localized excitons escape from traps to the mobility edge in the well and become again captured by deeper traps. That is, the exciton subsystem thermalizes to the lower energy states resulting in the low-temperature redshift of the PL maximum. When all deep impurity states are filled, increasing the temperature further leads to a population of the higher levels of the localized states. This population, in turn, results in the observed blueshift of the peak energy observed between 60 and 100 K in figure 6. A further increase in temperature redshifts the PL peak energy according to the Varshni equation. In order to represent this model in terms of rate equations let us introduce $D(E)$, $n_i(E)$ and $n(E_{me})$ as the DOS function in the band gap region, the population number of impurity states having energy, E , and the population number of the mobility edge state E_{me} , respectively. The rate equations [25–27] can be written as

$$\frac{dn}{dt} = G - \frac{n}{\tau_{nf}} - \int \frac{n(D(E) - n_i(E))}{\tau_c} dE + \int \frac{n_i(E)}{\tau_{te}} dE, \quad (7)$$

$$\frac{dn_i(E)}{dt} = + \frac{n(D(E) - n_i(E))}{\tau_c} - \frac{n_i(E)}{\tau_{te}} - \frac{n_i(E)}{\tau_{di}}. \quad (8)$$

Here, G is the free exciton generation rate in the well, and the rates, τ_c^{-1} , τ_{te}^{-1} , τ_{df}^{-1} and τ_{di}^{-1} are respectively the rates of exciton capture by traps, thermal activation from traps, free (in the well) exciton decay, and bound (in the well) exciton decay including radiative and non-radiative recombination. Using $D(E) \propto \exp\{-(E - E_0)^2/2\Delta^2\}$ with $E_0 = 1010$ meV, and $\Delta = 20$ meV derived from the PL data presented in figure 4(b) for sample 1 we can calculate the PL intensity as a function of temperature at various excitation intensity values. For a continuous wave excitation regime $dn/dt = dn_i(E)/dt = 0$, and we take $\tau_{te}^{-1}(T) = \tau_{te}^{-1}(0) \exp\{-(E_{me} - E)/k_B T\}$. Then, the expression for the PL intensity can be derived if one takes into account that the generation rate is given by $G = \sigma I_{ex}$ with σ being the absorption cross-section and I_{ex} the excitation intensity. Using $n_i(E, T, I_{ex})$ from equations (7) and (8), the PL intensity is reduced to

$$I_{PL}(T, I_{ex}) = A n_i(T, I_{ex}) \tau_{ri}^{-1}, \quad (9)$$

with A being a factor, which depends on the actual experimental arrangement. The best fit results received with

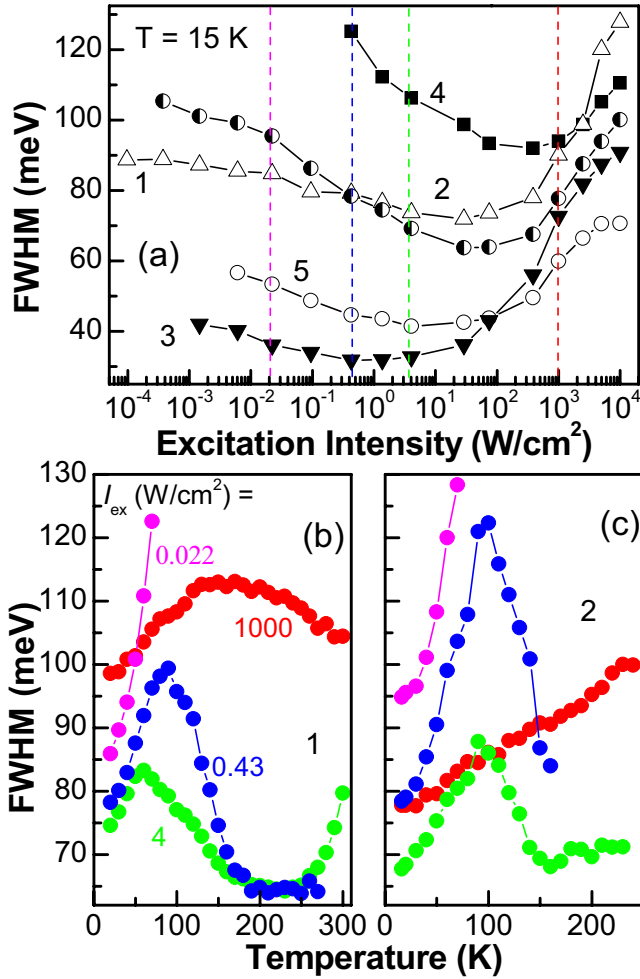


Figure 7. (a) FWHM measured at $T = 15$ K in all samples as a function of PL excitation density. Temperature dependences of PL FWHM measured under various excitation intensities in samples 1 (b) and 2 (c). Vertical lines in (a) delineate the intensities under which the temperature dependences shown in (b) and (c) with the same colour are measured.

$\tau_c^{-1} = 1.4 \times 10^6 \text{ cm}^2 \text{ s}^{-1}$, $\tau_{te}^{-1}(0) = 4.1 \times 10^{11} \text{ s}^{-1}$, $\tau_{df} = 3.8 \times 10^{15} \text{ s}^{-1}$ and $\tau_{di} = 3.1 \times 10^9 \text{ s}^{-1}$ are shown in figures 6(a) as dotted lines. Thus, modelling the two PL bands, i.e. the trap states and the QW states by Gaussians with intensities given by equation (9) we can reproduce the temperature dependence of the PL peak energy under various excitation intensities. It is clear that the vanishing of the S-shaped dependence under high excitation density is related to the filling of the defect sites even at low temperatures. There is a similar explanation for the anomalous behaviour of the FWHM with temperature increase measured under various excitation densities in samples 1 and 2. These dependences are shown in figure 7. At low excitation intensities the FWHM values increase in these samples. Such behaviour becomes understandable if one takes into account that the FWHM value has to be measured at the half-maximum of a single PL band. In samples 1 and 2 the single asymmetric PL band transforms to a doublet structure with the maxima of comparable strength separated at $T = 160$ K by ~ 160 meV. In this case the correct procedure requires band decomposition into separate PL components with a subsequent analysis of

each component. The low-energy sides of the PL bands in samples 1 and 2 are formed by the contribution of defect states with a finite number of allowed energy states; however, the weight of each component to the total PL band can be easily changed by changing the excitation intensity. At high excitation densities the contribution of the interband excitonic transition in the QW dominates, where the defect-related transitions are saturated and do not further influence the change in the PL spectral structure. It is clearly seen from figure 7 at the excitation of 1000 W cm^{-2} that the FWHM values monotonically increase in both samples giving evidence that the defects are saturated at a high excitation density and that the exciton dynamics are controlled by other mechanisms.

4. Conclusions

Summarizing, we carried out structural and optical studies of a set of high-quality single-layer $\text{GaAs}_{1-x}\text{Bi}_x/\text{GaAs}$ heterostructures with Bi concentration changing from 3.5% to 6.7%. High-resolution x-ray diffraction measurements and modelling were used to determine the composition and thickness of the QW layer. Transmission electron microscopy verified the high-quality, QW-like structure of the samples. Photoluminescence measurements were used to determine the energies of the transitions in the QW heterostructures as a function of the Bi concentration and thickness. The effects of quantum confinement were clearly demonstrated, thus establishing the nature of the intra-well optical transitions. The influence of material and structural disorder on the optical properties of the QWs was investigated. The nature of Bi-related defects was revealed to be different in the samples with Bi concentration less than 5% from those with concentration larger than 5%. A defect-related PL band was also shown to be present under slightly elevated temperatures. Also, it was demonstrated experimentally and verified theoretically that the variation of PL intensity and average energy as a function of temperature and excitation density is completely controlled by a competition of trap-related and inherent QW excitonic recombination. The identification and control of these traps would lead to improved predictability and overall usefulness of potential devices made of $\text{GaAs}_{1-x}\text{Bi}_x/\text{GaAs}$ QWs.

Acknowledgment

The authors acknowledge the financial support by the US National Science Foundation (NSF) via Grant No DMR-0520550 and MWN (Material World Network) Program between the NSF (Grant No DMR-1008107) and the Deutsche Forschungsgemeinschaft (Grant No Li 580/8-1). S-Q Yu acknowledges support by NSF Career Award No DMR-1149605.

References

- [1] Tiedje T, Young E C and Mascarenhas A 2008 *Int. J. Nanotechnol.* **5** 963
- [2] Lu X, Beaton D A, Lewis R B, Tiedje T and Zhang Y 2009 *Appl. Phys. Lett.* **95** 041903

- [3] Tixier S, Adamecyk M, Tiedje T, Francoeur S, Mascarenhas A, Wei P and Schiettekatte F 2003 *Appl. Phys. Lett.* **82** 2245
- [4] Tominaga Y, Kinoshita Y, Oe K and Yoshimoto M 2008 *Appl. Phys. Lett.* **93** 131915
- [5] Alberi K, Wu J, Walukiewicz W, Yu K M, Dubon O D, Watkins S P, Wang C X, Liu X, Cho Y-J and Furdyna J 2007 *Phys. Rev. B* **75** 045203
- [6] Tominaga Y, Oe K and Yoshimoto M 2010 *Appl. Phys. Express* **3** 062201
- [7] Ciatto G, Young E C, Glas F, Chen J, Alonso Mori R and Tiedje T 2008 *Phys. Rev. B* **78** 035325
- [8] Bertulis K, Krotkus A, Aleksejenko G, Pacebutas V, Andromavicius R and Molis G 2006 *Appl. Phys. Lett.* **88** 201112
- [9] Norman A G, France R and Ptak A J 2011 *J. Vac. Sci. Technol. B* **29** 03C121
- [10] Ciatto G, Thomasset M, Glas F, Lu X and Tiedje T 2010 *Phys. Rev. B* **82** R201304
- [11] Pettinari G, Engelkamp H, Christianen P C M, Maan J C, Polimeni A, Capizzi M, Lu X and Tiedje T 2011 *Phys. Rev. B* **83** 201201(R)
- [12] Ciatto G, Alippi P, Bonapasta A A and Tiedje T 2011 *Appl. Phys. Lett.* **99** 141912
- [13] Li C, Zeng Z O, Fan D S, Hirono Y, Wu J, Morgan T A, Hu X, Yu S Q, Wang Zh M and Salamo G J 2011 *Appl. Phys. Lett.* **99** 243113
- [14] Mazur Yu I, Dorogan V G, Schmidbauer M, Tarasov G G, Johnson S R, Lu X, Yu S-Q, Wang Zh M, Tiedje T and Salamo G J 2011 *Nanotechnology* **22** 375703
- [15] Imhof S *et al* 2010 *Appl. Phys. Lett.* **96** 131115
- [16] Pettinari G, Polimeni A, Blokland J H, Trotta R, Christianen P C M, Capizzi M, Maan J C, Lu X, Young E C and Tiedje T 2010 *Phys. Rev. B* **81** 235211
- [17] Mazur Yu I, Dorogan V G, Ware M E, Schmidbauer M, Tarasov G G, Johnson S R, Lu X, Yu S-Q, Tiedje T and Salamo G J 2013 *J. Appl. Phys.* submitted
- [18] Fafard S 1992 *Phys. Rev. B* **46** 4659
- [19] Singh J 1994 *Appl. Phys. Lett.* **64** 2694
- [20] Mohmad A R, Bastiman F, Hunter C J, Ng J S, Sweeney S J and David J P R 2011 *Appl. Phys. Lett.* **99** 042107
- [21] Rubel O, Galluppi M, Baranovskii S D, Volz K, Geelhaar L, Riechert H, Thomas P and Stolz W 2005 *J. Appl. Phys.* **98** 063518
- [22] Varshni Y P 1967 *Physica* **34** 149
- [23] Liang X G, Jiang D-S, Bian L-F, Pan Z, Li L-H and Wu R-H 2002 *Chin. Phys. Lett.* **19** 1203
- [24] Mazur Yu I, Dorogan V G, Bierwagen O, Tarasov G G, DeCuir E A Jr, Noda S, Zhuchenko Z Ya, Manaresreh M O, Masselink W T and Salamo G J 2009 *Nanotechnology* **20** 065401
- [25] Tarasov G G, Mazur Yu I, Zhuchenko Z Ya, Maaßdorf A, Nickel D, Tomm J W, Kissel H, Walther C and Masselink W T 2000 *J. Appl. Phys.* **88** 7162
- [26] Mazur Yu I, Liang B L, Wang Zh M, Guzun D, Salamo G J, Tarasov G G and Zhuchenko Z Ya 2006 *J. Appl. Phys.* **100** 054316
- [27] Mazur Yu I, Liang B L, Wang Zh M, Tarasov G G, Guzun D, Salamo G J, Mishima T D and Johnson M B 2006 *J. Appl. Phys.* **100** 054313
- [28] Wu Y-F, Lee J C, Nee T-E and Wang J-C 2011 *J. Lumin.* **131** 1267